Int. J. Nanosci. Nanotechnol., Vol. 16, No. 3, Sept. 2020, pp. 153-165

# Photocatalytic Degradation of Safranin Dye from Aqueous Solution Using Nickel Nanoparticles Synthesized by Plant Leaves

**Somayeh Heydari[1,*], Zahra Shirmohammadi Aliakbarkhani[2] and Mohadeseh Hosseinpour Zaryabi[3]**

[1]Department of Chemistry, University of Torbat-e jam, Torbat-e jam, Iran.
[2]Department of Water Engineering, University of Torbat-e Jam, Torbat-e Jam, Iran.
[3]Department of Chemistry, University of Birjand, Birjand, Iran.

(*) Corresponding author: so_heydari_83@yahoo.com
*(Received: 13 March 2019 and Accepted: 28 July 2019)*

***Abstract***

*In this paper, a facile and eco-friendly method for the preparation of Ni nanoparticles (Ni NPs) has been described based on the bioreduction of aqueous Ni(II) precursors with Phlomis cancellata Bunge extract. UV-visible spectrum of the aqueous medium containing Ni nanoparticles showed a peak of 390 nm. Since the experimental conditions of this procedure play vital roles in the synthesis rate of the NPs, a response surface methodology using the central composite design was employed for testing the reaction variables. The individual and interactive effects of process variables (temperature, time, concentration of $Ni(NO_3)_2$ and pH) upon extracellular biological synthesis of Ni NPs by Phlomis cancellata Bunge were studied. The statistical and perturbation plot analysis suggest that a reaction temperature of 90 °C, duration of 30 min., pH of 9.5 and concentration of 26 mM of $Ni(NO_3)_2$ would produce the highest amount of nanoparticles. The NPs were characterized by Scanning electron microscopy (SEM), energy dispersive X-ray spectroscopy (EDX), UV-Visible, and Infrared spectroscopy (IR). The SEM image of Ni NPs showed that the particle shape varied from spherical to polyhedral and ranged between 15 to 25 nm in size. These Ni NPs were studied for their potential role in photocatalytic degradation of safranin dye under solar light irradiation. At optimized conditions, up to 90% safranin dye degradation was achieved.*

***Keywords:*** *Photocatalytic degradation, Safranin, Phlomis cancellata Bunge, Nickel nanoparticles.*

## 1. INRODUCTION

In view of diverse applications of nanoparticles (NPs), the nanobiotechnology attract great extent of interests. NPs have attracted great attention due to their magnetic, thermal and catalytic properties revealing the fact that quantum effects turn out to be dominant and converting bulk material into nanoparticle, surface of volume size ratio changes [1-11]. In recent years, the photocatalytic systems based on nanoparticles have been widely used for removing pollutants [12-19]. In addition to many physical and chemical methods developed for preparing metallic NPs (such as lithography [20], laser ablation [21], high-energy irradiation [22], chemical reduction [23], electrochemistry [24], and photochemical reduction [25]), nanobiotechnology serves as a significant technique in order to make progress in clean, non-toxic and eco-friendly procedures for synthesis and assembly of metallic nanoparticles [26]. Utilizing biological organisms such as micro-organisms, plant extract or plant biomass is an alternative to chemical and physical methods to produce NPs in an eco-friendly manner. The plant extracts are widely employed for metal NP synthesis as they are easily available, safe, nontoxic and have a broad variety of metabolites such as flavonoids, polyphenols, alkaloids, and carotenoids aiding in reducing metal ions quicker than the microbe-mediated synthesis [27, 28]. Moreover, compared to microorganisms, the plant approach does

not need any special, complex, and multi-step procedures such as isolation, culture preparation, and culture maintenance.

Nickel nanoparticles (Ni NPs) attract great attention which might be due to their potential application in magnetic storage, biomedicine, catalyst, energy technology, and magnetically directionally targeting drug delivery [29]. They also find environmental applications in the field of adsorption of hazardous dye and inorganic pollutants and can be applied to treat textile and tannery effluents. [30].

Ni NPs are fabricated by various physico-chemical methods including i.e., seeding techniques [31], microemulsion [32], thermal decomposition [33], sol–gel [34], microwave heating [35], and sonochemical [36]. However, these techniques take prolonged time and are intensive in chemical or energy consumption and produce toxic reactive chemical that create environmental issue [37]. Recently, to overcome these problems, some green methods for synthesis of Ni NPs are reported using plant extracts. Pandian et al. synthesized Ni NPs using Ocimum sanctumleaf extract and presented that NiG as an economical, eco-friendly and efficient adsorbent in order to eliminate hazardous anionic pollutants and dyes from the aqueous [33]. Bibi et al. employed *Camellia Sinensis* (*C. Sinensis*) leaves extract to synthesize Ni NPs and evaluated their growth mechanism and photo-catalytic activity [38]. Synergistic anticancer effect of green synthesized Ni NPs and quercetin extracted from Ocimum sanctum leaf extract is proposed by Rameshthangam and Chitra [39]. Vasudeo and Pramod reported Biosynthesis of Ni NPs Using Leaf Extract of Coriander [40]. Sudhasree et al. drew a comparison between biological activity and toxicology of Ni NP synthesized through chemical and green procedures [41]. Desmodium gangeticum aqueous root extract was employed in order to prepare Ni NP without any stabilizing and reducing agent. There was no major significant difference in the nature of the NP prepared by both methods. However, green synthesized Ni NP indicated reduced size and superior monodispersity compared to chemical synthesized one.

Therefore, the eco-friendly approach to develop new photocatalysts and biological methods is desirable to eliminate or minimize environment hazardous since these methods are nonhazardous, cost effective and easy to apply at commercial scale [42-46].

Phlomis genus belongs to Labiatae (Lamiaceae) family with 70 annual and perennial species which disperse in the world, mostly in Asia [47]. Phlomis cancellata Bunge is an aperennial and annual species which can be applied more in modern medicine and different industries for its essential oil particulars. The phytochemical analysis of the Phlomis cancellata revealed that four major elements are identified in the herb essence such as Germacrene-D, β-Caryophyllene, Bicyclogermacrene, and β-selinene. Hexadecanoic acid and Germacrene-D compounds are recognised as the main elements in the herb essence.

Various physical and chemical parameters of the biosynthesis procedure, play important roles in the size, shape, and synthesis rate of the NPs. The present work was conducted to determine the optimum levels of reaction temperature, time duration and pH, as well as the concentration of $Ni(NO_3)_2$, for the green production of Ni NPs, by Phlomis cancellata Bunge extract using RSM and employing a central composite design Experimental.

## 2. EXPERIMENTAL

### 2.1. Materials and Instrumentation

Nickel nitrate $Ni(NO_3)_2$ analytical grade was purchased from Merck and used without further purification. Freshly prepared Double distilled deionized water was used throughout the experiment. Leaves of Phlomis cancellata Bunge were

collected from bakharz region of Khorasan state of Iran in month of April in the year 2017. UV-Visible double-beam spectro-photometer (Photonix Ar 2017, UV- Vis Array) with 1 nm resolution and optical length of 1 cm was used for measuring UV–Visible spectra of Ni NPs.

### 2.2. Preparation of Plant Aqueous Extract

Leaves of Phlomis cancellata Bunge were washed with deionized water thoroughly to remove the adhering soil and dust and dried at room temperature. The dried samples were powdered using a sterilized blade and stored until further analysis. 100 ml double deionized water was added to 1 g finely chopped leaves and boiled it at 80°C for 35 min and followed by filtering through filter paper to separate out the broth. The extract was stored at 4°C for further experiments.

### 2.3. Synthesis of Ni NPs by Phlomis Cancellata Bunge Extract

Ni NPs were synthesized by subjecting 0.1ml of Phlomis cancellata Bunge extract with aqueous 26 mmol·$L^{-1}$ nickle nitrate solution (pH:9.5) to the vigorous stirring in which reaction lasted for 1 h at 90 °C. The solution was freeze-dried for 24 h to obtain dried powder of nanoparticles. The formation of Ni NPs was monitored by using UV-Vis spectroscopy. The synthesis of Ni NPs can be explained in terms of the organic acids and heterocyclic compounds in the plant extract. These compounds play a key role in the synthesis process and can directly reduce Ni ions. In aqueous solution, nickle nitrate dissociates into negative nitrate anions and positive $Ni^{2+}$ cations as given in Fig. 1. The hydrated electrons from aqueous leaf extract of *Phlomis cancellata Bunge* reduce $Ni^{2+}$ cations into zero valent nickle ($Ni^0$) by nucleation process.

### 2.4. Characterization of Ni NPs

The spectra (UV–Visible) of Ni NPs were measured as a wavelength function by UV-Vis double-beam spectro-photometer (Photonix Ar 2017, UV- Vis Array).

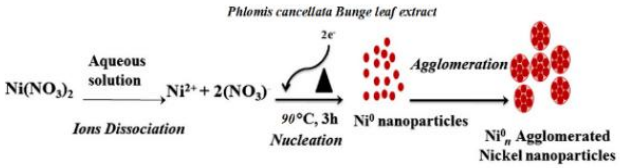


***Figure 1.*** *Ni NPs synthesis mechanism using Phlomis cancellata Bunge leaves extracts.*

After adding Phlomis cancellata Bunge extract to the aqueous solution of $Ni(NO_3)_2$ in experimental conditions, the solution was filled with quartz cell of path length 1 cm and UV-Vis spectral analysis has been carried out in the range of 300 to 800 nm. Deionized doubly distilled water was used as blank. Elemental analysis of the biosynthesized Ni NPs was studied using field emission Scanning Electron Microscope (SEM, TESCAN Mira3) operated at an accelerating voltage of 15 Kv. SEM provides detailed high resolution images of the sample by rastering a focused electron beam across the surface and detecting secondary or back scattered electron signal. In addition, an energy dispersive X-ray spectroscopy detector (EDX) was utilized to characterize the structures and composition of the NPs. Fourier Transformed Infrared (FTIR) spectrum of Phlomis cancellata Bunge extract and Ni NPs within the range of 400–4000 $cm^{-1}$ was recorded on Perkin Elmer 1750 FTIR Spectrophotometer. FT-IR analysis was performed, in order to determine the functional groups on Phlomis cancellata Bunge leaves extract and predict their role in the synthesis of Ni NPs. The spectrum describes the vibrations and rotations present in the nanoparticle in detail.

### 2.5. Statistical Analyses

Response surface methodology using central composite design was applied in order to optimize the levels of the most effective variables in Ni NPs biosynthesis

and to analyze their relationships. CCD argues for designing a full factorial by adding so-called star points (set points) and some number of replicate measurements at the center (center points). By spacing all the points at an equal distance from the center, a rotatable design is obtained giving each point equal amount in the process of estimating regression coefficients. So, the number of experiments decreases. Based on the one-factor experimental results, four critical variables selected were reaction time, nickel nitrate concentration, temperature, and reaction pH value. Every parameter was studied at different rational five coded levels, and the actual values for these codes are indicated in Table 1. The experiments were performed in three blocks of 36 sets of test conditions at five levels with one replicate and operated in a randomized arrangement to avoid systematic bias. The data analysis is carried out for each response variable described in the following sections as shown in Table. 2. The analysis of results was performed with statistical and graphical analysis software (Design Expert, Version 7.1.5 Trial). Design Expert software was applied for regression analysis of obtained data and to estimate regression equation coefficient.

The response surface models were fitted by means of least squares calculation using the following second-order polynomial equation.1:

$$Y = b_0 + \sum_{i=1}^{n} b_i X_i + \sum_{\substack{i=1 \\ j>i}}^{n-1} \sum_{j=2}^{n} b_{ij} X_i X_j + \sum_{i=1}^{n} b_{ii} X_i^2$$

where Y is the response variable to be modeled, $X_i$ and $X_j$ define the independent variables, $b_0$ is the constant coefficient, $b_i$ is the coefficient of linear effect, $b_{ij}$ is the coefficient of interaction effect, $b_{ii}$ the coefficients of quadratic effect and n is the number of variables.

### 2.6. Photo-Catalytic Procedure

The Photo-catalytic activity of Ni NPs was evaluated by degrading safranin dye (10 mL, 20 mg/L) containing 30 mg of Ni NPs. The degradation was conducted under solar light irradiation. The respective amount of dye solution (50 mL, 20 mg/L) was mixed with 30 mg of Ni NPs and the mixture was kept under stirring for 30 min in dark to bring the Ni NPs to constant equilibrium in the mixture. Then, the mixture was kept under sunlight. After 42 h, 3 mL sample was withdrawn and centrifuged at 10,000 rpm. Afterwards, the residual concentration of safranin dye was estimated (Photonix Ar 2017, UV- Vis Array) at 534 nm and percentage of dye degradation was calculated using relation shown in equation. 2.

$$\text{Decolorization } (\%) = \frac{(CO - Ce)}{CO} \times 100$$

where, $C_o$ is the initial concentration of dye, and $C_e$ is the concentration of dye at time "t" (after photocatalytic degradation).

## 3. RESULT AND DISCUSSION

### 3.1. Characterization of NiNPs

#### UV-Vis Spectrophotometry

Colour change was observed from blue to finally dark blue almost blackish blue colour indicating the formation of Ni NPs. Change in colour was due to excitation of surface plasmon resonance (SPR) which is characterized by UV-Vis spectroscopy indicating formation NPs. Fig. 2 illustrates the UV–Vis absorption spectra of synthesized nickel nanoparticles in Phlomis cancellata Bunge extract before and after synthesizing. The absorption spectrum of Ni NPs gives a peak centered at 390 nm proving the presence of nickel nanoparticles [48].

#### XRD Study

The X-ray diffraction pattern of Ni NPs is shown in Fig. 3. Typical characteristic diffraction peaks of Ni NPs emerge at 2 theta = 38.74°, 42.60°, 60.23° and 78.68° confirmed the formation of face –centered cubical Ni. The pattern is in accordance with Joint Committee on Power Diffraction Standards (JCPDS) file (card number 04-0835).

***Table 1.*** *The levels employed for the different factors employed by experimental investigations.*

| Name | $-\alpha$ | -1 | 0 | +1 | $+\alpha$ |
|---|---|---|---|---|---|
| pH | 2 | 4.5 | 7 | 9.5 | 12 |
| Tem($^{\circ}$C) | 25 | 50 | 75 | 100 | 125 |
| Time(min) | 15 | 30 | 45 | 60 | 75 |
| $C_{Ni(NO3)2}$ (mM) | 5 | 12 | 19 | 26 | 33 |

***Table 2.*** *Surface regression procedure.*

| Run | Block | Factor1 A:pH | Factor 2 B: Tem. | Factor 3 C: Time | Factor 4 D:$C_{Ni(NO3)2}$ | Response1 Absorbance |
|---|---|---|---|---|---|---|
| 1 | Block 1 | 7 | 75 | 45 | 19 | 0.85 |
| 2 | Block 1 | 4.5 | 50 | 30 | 26 | 0.66 |
| 3 | Block 1 | 4.5 | 100 | 60 | 26 | 0.57 |
| 4 | Block 1 | 9.5 | 100 | 30 | 26 | 1.51 |
| 5 | Block 1 | 4.5 | 50 | 60 | 12 | 1.45 |
| 6 | Block 1 | 9.5 | 100 | 60 | 12 | 0.47 |
| 7 | Block 1 | 4.5 | 100 | 30 | 12 | 0.38 |
| 8 | Block 1 | 7 | 75 | 45 | 19 | 0.82 |
| 9 | Block 1 | 9.5 | 50 | 30 | 12 | 0.60 |
| 10 | Block 1 | 9.5 | 50 | 60 | 26 | 0.97 |
| 11 | Block 2 | 4.5 | 100 | 60 | 12 | 0.84 |
| 12 | Block 2 | 9.5 | 50 | 60 | 12 | 0.95 |
| 13 | Block 2 | 4.5 | 50 | 30 | 12 | 0.19 |
| 14 | Block 2 | 4.5 | 100 | 30 | 26 | 0.68 |
| 15 | Block 2 | 7 | 75 | 45 | 19 | 0.79 |
| 16 | Block 2 | 9.5 | 100 | 30 | 12 | 0.60 |
| 17 | Block 2 | 9.5 | 100 | 60 | 26 | 0.34 |
| 18 | Block 2 | 7 | 75 | 45 | 19 | 0.85 |
| 19 | Block 2 | 9.5 | 50 | 30 | 26 | 1.25 |
| 20 | Block 2 | 4.5 | 50 | 60 | 26 | 0.90 |
| 21 | Block 3 | 7 | 75 | 45 | 19 | 0.88 |
| 22 | Block 3 | 7 | 75 | 45 | 33 | 0.57 |
| 23 | Block 3 | 7 | 75 | 45 | 19 | 0.79 |
| 24 | Block 3 | 7 | 75 | 45 | 19 | 0.82 |
| 25 | Block 3 | 12 | 75 | 45 | 19 | 0.90 |
| 26 | Block 3 | 2 | 75 | 45 | 19 | 0.69 |
| 27 | Block 3 | 7 | 75 | 75 | 19 | 1.08 |
| 28 | Block 3 | 7 | 75 | 15 | 19 | 0.90 |
| 29 | Block 3 | 7 | 45 | 45 | 19 | 0.88 |

| | | | | | | |
|---|---|---|---|---|---|---|
| 30 | Block 3 | 7 | 75 | 45 | 19 | 0.79 |
| 31 | Block 3 | 7 | 125 | 45 | 19 | 0.52 |
| 32 | Block 3 | 7 | 75 | 45 | 19 | 0.82 |
| 33 | Block 3 | 7 | 75 | 45 | 19 | 0.85 |
| 34 | Block 3 | 6 | 75 | 45 | 5 | 0.19 |
| 35 | Block 3 | 6 | 75 | 45 | 19 | 0.88 |
| 36 | Block 3 | 6 | 25 | 45 | 19 | 0.90 |

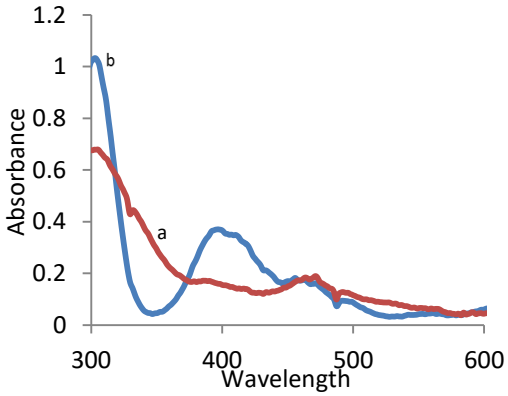


***Figure 2.*** *UV-Visible spectra of synthesized Ni NPs in Phlomis cancellata Bunge extract (a) before synthesized (b) after synthesized.*

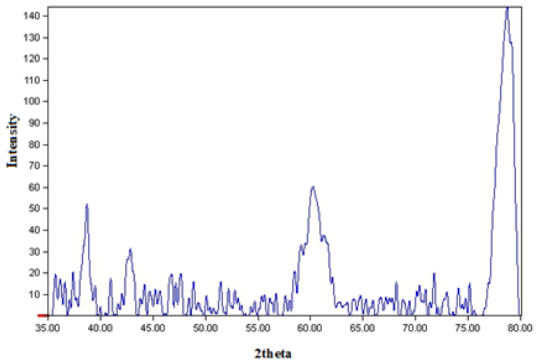


***Figure 3.*** *XRD pattern of Ni NPs.*

***SEM and EDX Analysis***

SEM micrograph for the biosynthesized Ni NPs obtained by mediation of Phlomis cancellata Bunge is represented in Fig. 4. The SEM image of Ni NPs shows that the particle shape varied from spherical to polyhedral and the particle size ranged between 15 and 25 nm. According to Govindasamy et al [49], the surface morphology of Ni NPs was irregular polygonal, cylindrical and spherical in shapes. To further understand the synthesis of Ni NPs, the existence of nickel element in the biosynthesized Ni NPs was confirmed by EDX as exhibited in Fig. 5, which contains intense peaks of C, O, N and Ni, confirming the presence of Ni. The C, O and N signals are attributed mainly to the polyphenol groups and other C, N, O-containing molecules in Phlomis cancellata Bunge leaf extracts. Specifically, the C, N, O and Ni loading of Ni NPs is 27.03 wt%, 8.55 wt%, 53.91 and 10.51 wt%, respectively.

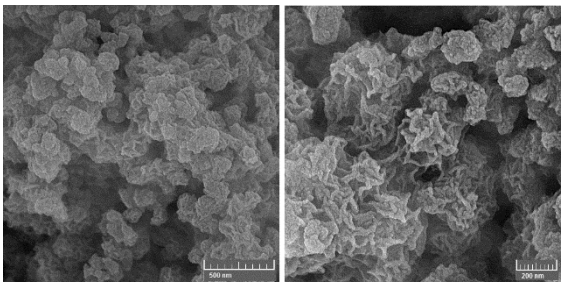

***Figure 4.*** *SEM image of Ni NPs.*

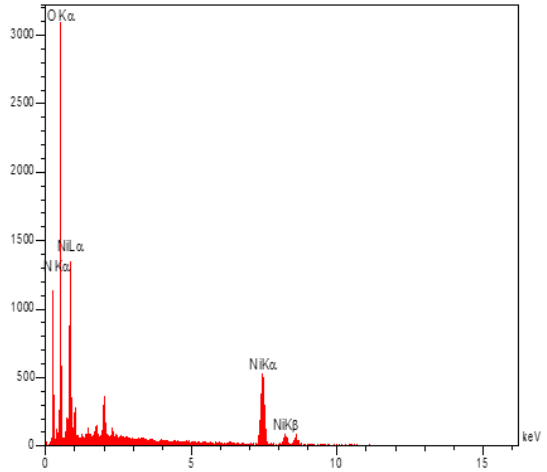


***Figure 5.*** *EDX spectrum obtained for Ni NPs.*

**FTIR Spectroscopy**

The binding properties of Ni NPs using Phlomis cancellata Bunge extract were investigated by FTIR spectroscopic analysis. The functional groups may be responsible for Ni NPs biosynthesis, stabilization, and capping. The FTIR spectrum of Phlomis

cancellata Bunge extract and Ni NPs produced by Phlomis cancellata Bunge mediation are represented in Fig. 6a and b. The peaks observed in the region between 1000 and 1700 $cm^{-1}$can be assigned to hydroxyl and carbonyl groups and –C–O and –C–O–C stretching modes through the obtained spectrum. On the other hand, methoxy, methylene, and methyl groups stretching vibrations via C–H could be detected at 2919, and 2851 $cm^{-1}$, whereas stretching of O–H in flavonoids, alcohols, and phenols was observed at 3404 $cm^{-1}$. The peak at 1633 $cm^{-1}$ is attributed to N–H bend primary amines. The peak at 1430 $cm^{-1}$ indicates C–C stretch (in ring) in aromatics. The FTIR analysis evidences the presence of N–H, C–O, C–H and O–H groups corresponding to presence of metabolites and proteins surrounding the Ni NPs. Mallikarjuna et al. suggested that the carbonyl and hydroxyl groups from amino acid residues or proteins can strongly bind to metal nanoparticles like capping agent and stabilize the nanoparticles in the aqueous medium [50].

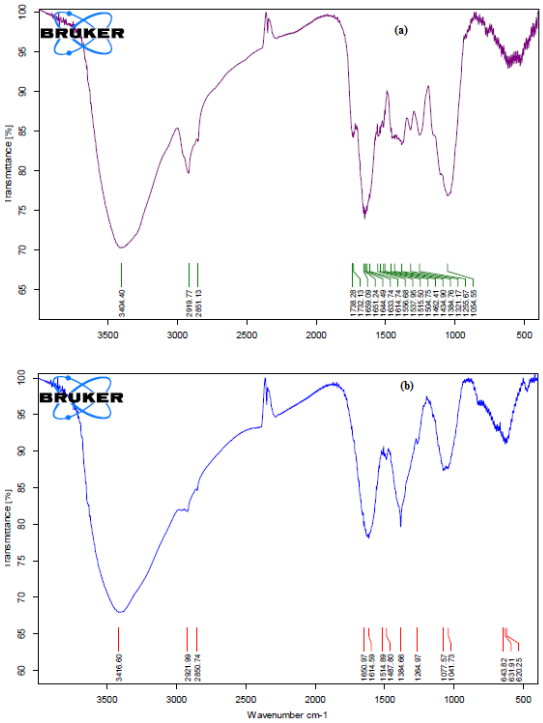


***Figure6.*** *FTIR spectrum of Ni NPs, (a) extract, (b) extract with Ni.*

### 3.2. Experimental Design

In this study, the effect of four factors, concentration of $Ni(NO_3)_2$, pH level, temperature and time, on the biosynthesis of Ni NPs was investigated. To find the most suitable fitting of the experimental data, a response surface model was developed using the regression analysis by considering different combinations of the linear, quadratic and interaction terms in polynomial equations which may be expressed as the following equation: (1).

$$R = -3.98905 + 0.17021 \times pH + 0.020378 \times Tem + 0.089654 \times Time + 0.14050 \times C_{Ni\ (NO3)2} - 1.10720E\text{-}004 \times pH \times Tem - 5.14358E\text{-}003 \times pH \times Time + 5.35212E\text{-}003 \times pH \times C_{Ni\ (NO3)2} - 4.23640E\text{-}004 \times Tem \times Time + 7.84809E\text{-}005 \times Tem \times C_{Ni\ (NO3)2} - 1.95183E\text{-}003 \times Time \times C_{Ni\ (NO3)2} - 5.71974E\text{-}004 \times pH^2 - 3.94931E\text{-}005 \times Tem^2 + 1.99668E\text{-}004 \times Time^2 - 2.18611E\text{-}003 \times C_{Ni\ (NO3)2}$$

The adequacy of each model was checked using the F-values, lack of fit, and $R^2$-values, and finally a quadratic model was adopted. The statistical significance of the full quadratic models predicted was considered by the analysis of variance (ANOVA). The ANOVA results of the quadratic model are summarized in Table 3.

The regression model resulted in a determination coefficient ($R^2$ = 0.9887), indicating that only 0.0113% of the variation can't be explained by the model. The adjusted determination coefficient at adjusted-$R^2$ = 0.9803, confirmed that the model was highly significant. Additionally, the prediction R-squared of 0.9637 was in acceptable agreement with the R-squared and demonstrated a high predictive power of model. Adequate Precision measures the signal to noise ratio. A ratio greater than 4 is desirable. Our ratio of 46.279 indicates an adequate signal. This model can be used to navigate the design space.

Fig. 7a-f shows 3D response surfaces and contour plots of the model. The responses were mapped against two experimental factors while the other factors are held constant at its central level. The signs and the magnitude of the factors is estimated for each variable and quadratic interaction

is also determined. Unless otherwise stated, the significance level employed in the analysis was 5%. Additionally, interactions between the variables can also be clearly seen from the perturbation plot in Figure. 8, which came up by default from the design expert software and perturbation theory using mathematical methods for finding an optimized condition to synthesize of Ni NPs. The statistical and perturbation plot analysis suggest that a reaction temperature of 90 °C, duration of 30 min., pH of 9.5 and concentration of 26 mM of $Ni(NO_3)_2$ would produce the highest amount of nanoparticles.

***Table 3.*** *The ANOVA results of the quadratic model.*

| Source | Sum of Squares | Degree of Freedom | Mean Square | F-Value | P-Value Prob > F | |
|---|---|---|---|---|---|---|
| Block | 0.040 | 2 | 0.020 | | | |
| Model | 2.81 | 14 | 0.20 | 118.47 | <0.0001 | Significant |
| A-pH | 0.087 | 1 | 0.087 | 51.48 | <0.0001 | |
| B-Tem | 0.23 | 1 | 0.23 | 134.09 | <0.0001 | |
| C-Time | 0.041 | 1 | 0.041 | 24.27 | <0.0001 | |
| D-$C_{Ni(NO3)2}$ | 0.20 | 1 | 0.20 | 116.13 | <0.0001 | |
| AB | 7.662E-004 | 1 | 7.6620E-004 | 0.45 | 0.5096 | |
| AC | 0.60 | 1 | 0.60 | 350.94 | <0.0001 | |
| AD | 0.14 | 1 | 0.14 | 82.75 | <0.0001 | |
| BC | 0.40 | 1 | 0.40 | 238.07 | <0.0001 | |
| BD | 3.018E-003 | 1 | 3.018E-003 | 1.76 | 0.1980 | |
| CD | 0.67 | 1 | 0.67 | 396.19 | <0.0001 | |
| $A^2$ | 3.979E-004 | 1 | 3.979E-004 | 0.23 | 0.6337 | |
| $B^2$ | 0.019 | 1 | 0.019 | 11.16 | 0.0034 | |
| $C^2$ | 0.063 | 1 | 0.063 | 37.05 | <0.0001 | |
| $D^2$ | 0.36 | 1 | 0.36 | 210.62 | <0.0001 | |
| Residual | 0.032 | 19 | 1.696E-003 | | | |
| Lack of Fit | 0.019 | 10 | 1.929E-003 | 1.34 | 0.3345 | not significant |
| Pure Error | 0.013 | 9 | 1.438E-003 | | | |
| Core Total | 2.89 | 35 | | | | |

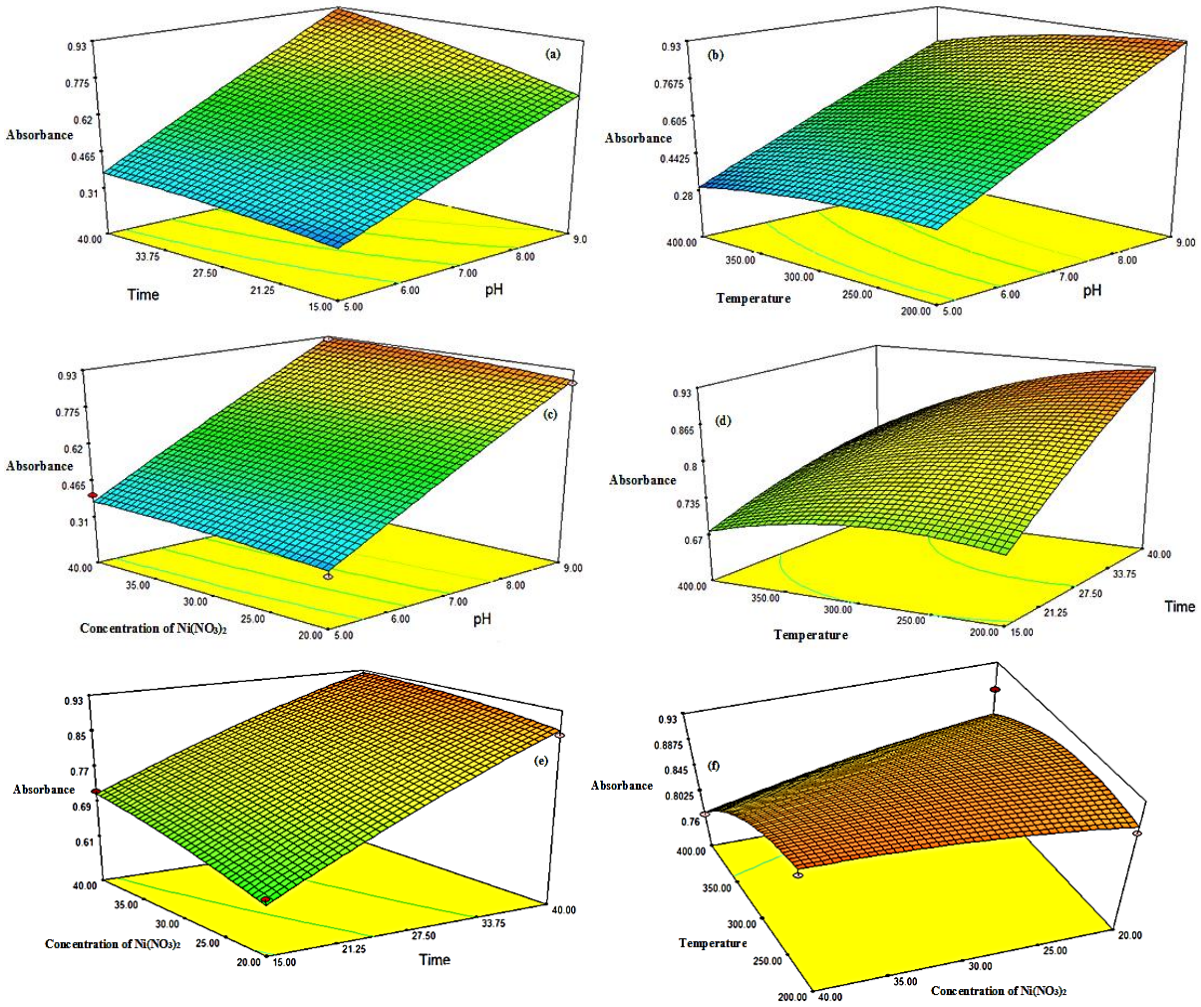


***Figure 7.*** *Estimated response surfaces with related contours by plotting absorbance versus (a) pH and Time of reaction; (b) pH and Temperature; (c) $Ni(NO_3)_2$ concentration and pH; (d) Temperature and Time of reaction; (e) $Ni(NO_3)_2$ concentration and Time of reaction; (f) Temperature and $Ni(NO_3)_2$ concentration.*

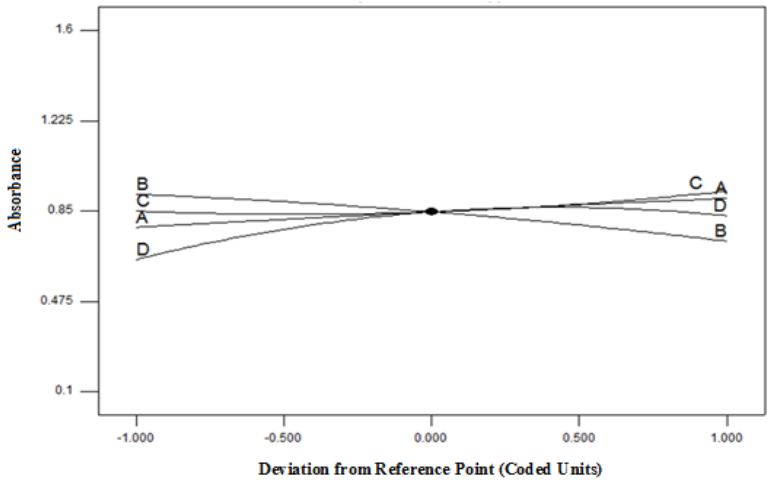


***Figure 8.*** *Perturbation plot of Ni NPs yield optimization.*

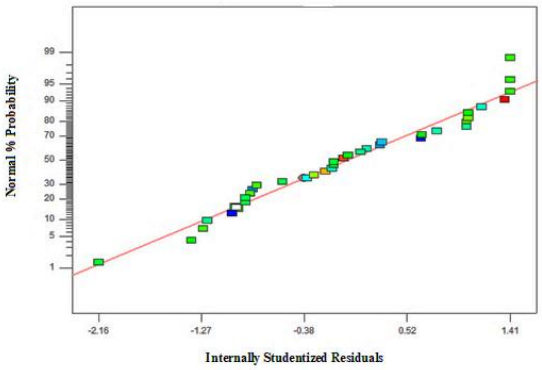


***Figure 9.*** *Normal plot of residuals (Internally Studentized Residuals).*

Table 3 presented F value and p-value of the variables included in the model. F value compares the mean square with the residual mean square. The model F-value implies the model is significant. P-value (Prob > F) is the probability of seeing the observed F value and a parameter to see if the null hypothesis is true (there are no factor effects). A P-value lower than 0.0001 was found, demonstrating again the high significance of the regression model. A p-value less than 0.05 in the ANOVA Table indicates the statistical significance of an effect at 95% confidence level. The data in Table 3 indicate that factors A, B, C, D and quadratic terms of C and D are significant model terms.

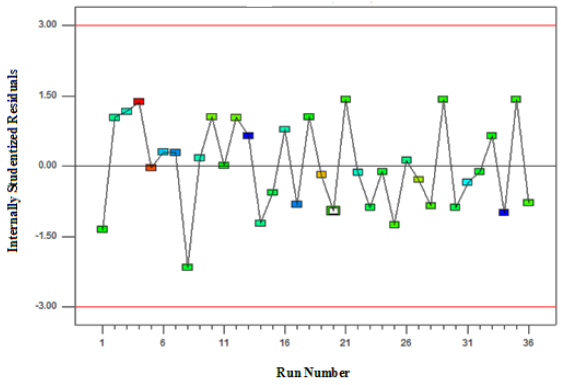


***Figure 10.*** *Residual vs. Run (Internally Studentized Residuals).*

The interactions between the time of reaction with the other three factors (pH, temperature and concentration of $Ni(NO_3)_2$) and the interactions between the pH and the concentration of $Ni(NO_3)_2$ are statistically significant. While the interactions between the temperature with the pH, and the concentration of $Ni(NO_3)_2$ are statistically insignificant. As it is noticeable, the F-value of lack of fit (LOF) of 1.34 indicated that the LOFs were not significant relative to the pure errors. Figure 9 shows the normal probability plot of the residuals which reveals the systematic deviations from the expectations. The residuals are normally distributed if the points on the plot follow a straight line [51]. The probability plot of the studentized residuals is to check for normality of residuals. As shown in Figure 10, all the internally studentized residual were randomly scattered across the graph and furthermore, there is no significant distribution pattern for all the diagnostics plots. The red line was produced by the software based on the internally studentized to define outliers, as displayed in the diagnostics plots outlier exists in the plot indicating that the model is consistent with all the data.

### 3.3. Photo-catalytic Activity of NiNPs

The Photo-catalytic activity of Ni NPs was evaluated by degrading safranin dye (10 mL, 20 mg/L) containing 30 mg of Ni NPs under solar light irradiation for 42 h. The percentage degradation of safranin is illustrated in Fig. 11. As it is conspicuous,

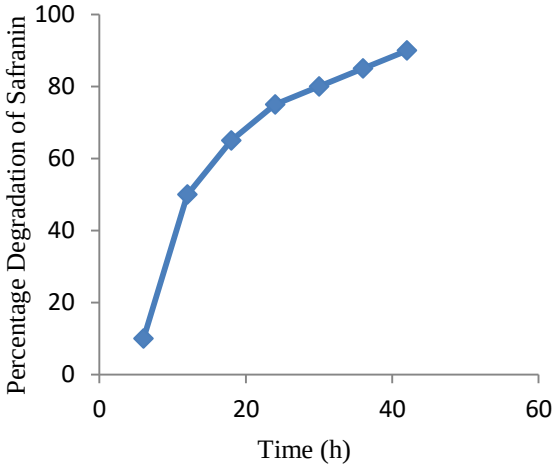


***Figure 11.*** *Percentage degradation of safranin dye as a function of solar light irradiation exposure time (dye*

*concentration 20 mg/L, Ni NPs dose 30 mg)*

the safranin dye degradation increased gradually with irradiation time and after 42 h of irradiation, 90% safranin dye degradation was achieved. The probable mechanism of degradation could be attributed to the photocatalytic active sites that created on the surface of catalyst when exposed to light and electron jumps from valence band to conduction band leaving behind $h^+$, which converts water molecule into $H^+$ and •OH radical [52]. The •OH radical degrade the safranin molecule into oxidative by-products and finally, into low molecular weight organic acid and inorganic ions. On the other hand, the oxygen converted into superoxide anion radical ($O_2$•$^-$) by absorbing electron, which also produce •OH radical. Hence, it is evident that Ni NPs synthesized from Phlomis cancellata Bunge extract is highly potential photocatalytic agent for dye degradation in the presence of sunlight.

## 3. CONCLUSION

The present work describes a cheaper, ecofriendly and simple route for biosynthesis of Ni NPs using Phlomis cancellata Bunge extracts. Since the experimental conditions of this procedure play vital roles in the synthesis rate of the NPs, a response surface methodology using the central composite design was employed for testing the reaction variables. The optimized conditions for high yield of Ni NPs synthesis are 26 mM $Ni(NO_3)_2$ with 30 min duration time, reaction temperature of 90°C and pH of 9.5. The UV–Vis absorption peak was monitored at 395 nm. Microscopic studies by SEM showed that the particle shape varied from spherical to polyhedral and the particle size ranged between 15 and 25 nm. The Ni NPs showed high catalytic activity for degradation of safranin dye under the sunlight. This photocatalytic treatment is highly efficient versus other physico-chemical treatment methods for the degradation of dyes in textile wastewater and other toxic pollutants. Novelty of this present study is that the plant extract is very cost effective, eco-friendly, economic and effective alternative for the large scale synthesis of Ni NPs. However, applying *Phlomis cancellata* leaves can add value to a non-usable waste.


## ACKNOWLEDGEMENT

The authors acknowledge the financial support of this work by University of Torbat-e jam, Torbat-e jam, Iran.


## REFERENCES


1. Remya, V. R, Abitha, V. K., Rajput, P. S., Rane, A. V., Dutta, A., (2017). " Silver nanoparticles green synthesis: a mini review", *Chem. Int*., 3: 165-171.
2. Monsef Khoshhesab, Z., Ayazi, Z., Dargahi M., (2020). "Synthesis of Magnetic Graphene Oxide Nanocomposite for Adsorption Removal of Reactive Red 195: Modelling and Optimizing via Central Composite Design", *Int. J. Nanosci. Nanotechnol*., 16: 35-48
3. Tawfik A. Saleh., Vinod K. Gupta., (2012). "Photo-catalyzed degradation of hazardous dye methyl orange by use of a composite catalyst consisting of multi-walled carbon nanotubes and titanium dioxide", *J. Colloid Interface Sci*., 371: 101-106.
4. Zeinali, S; Tatian, S., (2019). "Vanadium Removal from Fuel Oil and Waste Water in Power Plant Using Humic Acid Coated Magnetic Nanoparticles", *Int. J. Nanosci. Nanotechnol*., 15: 249-263.
5. Devaraj, M., Saravanan, R., Deivasigamani, R. K., Gupta, V. K., Jayadevan, S., (2016). "Fabrication of novel shape Cu and $Cu/Cu_2O$ nanoparticles modified electrode for the determination of dopamine and paracetamol", *J. Mol. Liq*., 221: 930-941.
6. Saravanan, R., Joicy, S., Gupta, V. K., Narayanan, V., Stephen, A., (2013). "Visible light induced degradation of methylene blue using $CeO_2/V_2O_5$ and $CeO_2$/CuO catalysts", *Mater. Sci. Eng. C*., 33, 4725-4731.
7. Saravanan, R., Karthikeyan, N., Gupta, V. K., Thirumal, E., Stephen, A., (2013). "ZnO/Ag nanocomposite: An efficient catalyst for degradation studies of textile effluents under visible light", *Mater. Sci. Eng. C*., 33: 2235-2244.

8. Gupta, V. K., Atar, N., Yola, M. L., Zafer Ustundag, Z., Uzun, L., (2014). "A novel magnetic Fe@Au coreeshell nanoparticles anchored graphene oxide recyclable nanocatalyst for the reduction of nitrophenol compounds", *Water. Res*., 48: 210-217.
9. Yola, M. L., Gupta, V. K., Eren, T., Sen, A. E., Atar, N., (2014). "A novel electro analytical nanosensor based on graphene oxide/silver nanoparticles for simultaneous determination of quercetin and morin", *Electrochim. Acta*., 120: 204-211.
10. Vanaja, A; Suresh, M; Jeevanandam, J., (2019). "Facile Magnesium Doped Zinc Oxide Nanoparticle Fabrication and Characterization for Biological Benefits", *Int. J. Nanosci. Nanotechnol*., 15: 277- 286.
11. Ghaedi, M., Hajjati, S., Mahmudi, Z., Tyagi, I., Gupta, V. K., (2015). "Modeling of competitive ultrasonic assisted removal of the dyes – Methylene blue and Safranin-O using $Fe_3O_4$ nanoparticles", *Chemical Eng. J*., 268: 28-37.
12. A. Banisharif, A., Hakim Elahi, S., Anaraki Firooz, A., Khodadadi, A. A., Mortazavi, Y., (2013). "$TiO_2$/$Fe_3O_4$ Nanocomposite Photocatalysts for Enhanced Photo-Decolorization of Congo Red Dye", *Int. J. Nanosci. Nanotechnol*., 9: 193-202.
13. Saravanan, R., Sacari, E., Gracia, F., Mansoob Khan, M., Gupta, V. K., (2016). "Conducting PANI stimulated ZnO system for visible light photocatalytic degradation of coloured dyes", *J. Mol. Liq*., 221: 1029-1033.
14. Rajendran, S., Mansoob Khan, M., Gracia, F., Qin, J., Gupta, V. K., Arumainathan, S., (2016). "$Ce^{3+}$-ion-induced visible-light photocatalytic degradation and electrochemical activity of ZnO/$CeO_2$ nanocomposite", *Sci. Rep*., 6: 1-11.
15. Saravanan, R., Karthikeyan, S., Gupta, V. K., Sekaran, G., Stephen, A., (2013). "Enhanced photocatalytic activity of ZnO/CuO nanocomposite for the degradation of textile dye on visible light illumination", *Mater. Sci. Eng. C*., 33: 91-98.
16. Saravanan, R., Thirumal, E., Gupta, V. K., Narayanan, V., Stephen, A., (2013). "The photocatalytic activity of ZnO prepared by simple thermal decomposition method at various temperatures", *J. Mol. Liq*., 177: 394-401.
17. Saravanan, R., Gupta, V. K., Prakash, T., Narayanan, V., Stephen, A., (2013). "Synthesis, characterization and photocatalytic activity of novel Hg doped ZnO nanorods prepared by thermal decomposition method", *J. Mol. Liq*., 178: 88-93.
18. Narayan, H., Alemu, H., (2017). "A Comparison of Photocatalytic Activity of $TiO_2$ Nanocomposites Doped with $Zn^{2+}$/$Fe^{3+}$ and $Y^{3+}$ Ions", *Int. J. Nanosci. Nanotechnol*., 13: 315-325.
19. Saleh, T. A., Gupta, V. K., (2011). "Functionalization of tungsten oxide into MWCNT and its application for sunlight-induced degradation of rhodamine B", *J. Colloid. Interface. Sci*., 362: 337-344.
20. Huang, X., Ratchford, D., Pehrsson, P. E., Yeom, J., (2016). "Fabrication of metallic nanodisc hexagonal arrays using nanosphere lithography and two-step lift-off", *Nanotechnol*., 27: 395302-395309.
21. Kim, M., Osone, S., Kim, T., Higashi, H., Seto, T., (2017). "Synthesis of Nanoparticles by Laser Ablation: A Review", *KONA Powder Part J*., 34: 80-90.
22. Tsukuda, S., Takahasi, R., Seki, S., Sugimoto, M., Idesaki, A., Yoshikawa, M., Tanaka, S. I., (2016). "Fabrication of Pt nanoparticle incorporated polymer nanowires by high energy ion and electron beam irradiation", *Radiat. Phys. Chem*., 118: 16-20.
23. Khan, A., Rashid, A., Younas, R., Chong, R., (2016). "A chemical reduction approach to the synthesis of copper nanoparticles", *Int Nano Lett*., 6: 21-26.
24. Ahmadi, R., Razaghian, A., Eivazi, Z., Shahidi, K., (2018). "Synthesis of Cu-CuO and Cu-$Cu_2O$ Nanoparticles via Electro-Explosion of Wire Method", *Int. J. Nanosci. Nanotechnol*., 14: 93-99.
25. Eustis, S., Hsu, H. Y., El-Sayed, M. A., (2005). "Gold nanoparticle formation from photochemical reduction of $Au^{3+}$ by continuous excitation in colloidal solutions. A proposed molecular mechanism", *J. Phys. Chem. B.*, 109: 4811-4815.
26. Salata, O. V., (2004). "Applications of nanoparticles in biology and medicine", J. Nanobiotechnol., 2: 1-6.
27. Lima, A. K. O; Vasconcelos, A. A; Sousa Junior, J. J. V; Escher, S. K. S; Nakazato, G; Taube Junior, P.S., (2019). "Green Synthesis of Silver Nanoparticles Using Amazon Fruits", *Int. J. Nanosci. Nanotechnol*., 15: 179-188.
28. Karatoprak, G. S., Aydin, G., Altinsoy, B., Altinkaynak, C., Koşar, M., Ocsoy, I., (2017). "The Effect of Pelargonium endlicherianum Fenzl. root extracts on formation of nanoparticles and their antimicrobial activities", *Enz. Microb. Technol*., 97: 21-26.
29. Liu, S., Mei, J., Zhang, C., Zhang, J., Shi, R., (2017). "Synthesis and magnetic properties of shuriken-like nickel nanoparticles", *J. Mater. Sci. Technol*., 34: 836- 341.
30. Pandian, C. J., Palanivel, R., Dhananasekaran, S., (2015). "Green synthesis of nickel nanoparticles using Ocimum sanctum and their application in dye and pollutant adsorption", *Chin. J. Chem. Eng*., 23: 1307-1315.

31. Prieto, P., Nistor, V., Nouneh, K., Oyama, M., Abd-Lefdil, M., Diaz, R., (2012). "XPS study of silver, nickel and bimetallic silver-nickel nanoparticles prepared by seed-mediated growth", *Appl. Surf. Sci*., 258: 8807- 8813.
32. Sharma, P., Singh, S., Virk, H. S., (2010). "Formation of CdS Nanoparticles in Microemulsion Using Different Co-surfactant and Water to Surfactant Molar Ratio", *Int. J. Nanosci. Nanotechnol*., 6: 236-243.
33. Hou, Y., Gao, S., (2003). "Monodisperse nickel nanoparticles prepared from a monosurfactant system and their magnetic properties", *J Mater Chem*., 13: 1510- 1512.
34. Mohd Zorkipli, N. N., Mohd Kaus, N. H., Mohamad, A. A., (2016). "Synthesis of NiO Nanoparticles through Sol-gel Method", *Procedia Chem*., 19: 626- 631.
35. Eluri, R., Paul, B., (2012). "Microwave assisted greener synthesis of nickel nanoparticles using sodium hypophosphite", *Mater. Lett*., 76: 36-39.
36. Abu-Much, R., Gedanken, A., (2008). "Sonochemical Synthesis under a Magnetic Field: Fabrication of Nickel and Cobalt Particles and Variation of Their Physical Properties", *Chem Eur J.*, 14: 10115-10122.
37. Nouren, S., Bhatti, H. N., Iqbal, M., Bibi, I., Kamal, S., Sadaf, S., Sultan, M., Kausar, A., Safa, Y., (2017). " By-product identification and phytotoxicity of biodegraded Direct Yellow 4 dye", *Chemosphere.*, 169: 474-484.
38. Bibi, I., Kamal, S., Ahmed, A., Iqbal, M., Nouren, S., Jilani, K., Nazar, N., Amir, M., Abbas, A., Ata, S., Majid, F., (2017). "Nickel nanoparticle synthesis using Camellia Sinensis as reducing and capping agent: Growth mechanism and photo-catalytic activity evaluation", *Int J Biol Macromol*., 103: 783-790.
39. Rameshthangam, P., Chitra, J. P., (2018). "Synergistic anticancer effect of green synthesized nickel nanoparticles and quercetin extracted from Ocimum sanctum leaf extract", *J. Mater. Sci. Technol*., 34 (3): 508-522.
40. Vasudeo, K., Pramod, K., (2016). "Biosynthesis of Nickel Nanoparticles Using Leaf Extract of Coriander", *Biotechnol Ind J*., 12: 106- 111.
41. Sudhasree, S., Mahalakshmi, S., Brindha, P., Kurian, G., (2014). "Synthesis of nickel nanoparticles by chemical and green route and their comparison in respect to biological effect and toxicity", *Toxicol. Environ. Chem.*, 96: 743-754.
42. Mittal, D., Narang, K., Leekha Kapinder, A., Kumar, K., Verma, A. K., (2019). "Elucidation of Biological Activity of Silver Based Nanoparticles Using Plant Constituents of Syzygium cumini", *Int. J. Nanosci. Nanotechnol*., 15: 189-198.
43. Gupta, V. K., Nayak, A., Agarwal, S., (2015). "Bioadsorbents for remediation of heavy metals: Current status and their future prospects", *Environ. Eng. Res*., 20: 1-18.
44. Pal, S., Mondal, S., Maity, J., Mukherjee, R., (2018). "Synthesis and Characterization of ZnO Nanoparticles using Moringa Oleifera Leaf Extract: Investigation of Photocatalytic and Antibacterial Activity", *Int. J. Nanosci. Nanotechnol*., 14: 111-119.
45. Gupta, V. K., Ali, I., Saleh, T. A., Siddiqui, M. N., Agarwal, S., (2013). "Chromium removal from water by activated carbon developed from waste rubber tires", *Environ. Sci. Pollut. Res*., 20: 1261-1268.
46. Gupta, V. K., Suhas., Tyagi, I., Agarwal, S., Singh, R., Chaudhary, M., Harit, A., Kushwaha, S., (2016). " Column operation studies for the removal of dyes and phenols using a low cost adsorbent", *Global J. Environ. Sci*. *Manage*., 2: 1-10.
47. Hasani-Ranjbar, Sh., Larijani, B., Abdollahi. M., (2008). "A systematic review of Iranian medicinal plants useful in diabetes mellitus", *Arch. Med. Sci*., 4: 285-292.
48. Khalid, N., Munetaka, O., Raquel, D., Mohammed, A., Kityk, I. V., Mosto, B., (2011). "Nanoscale synthesis and optical features of metallic nickel nanoparticles by wet chemical approaches", *J. Alloys Compd*., 509 (19): 5882-5886.
49. Govindasamy, R., Jeyaraman, R., Kadarkaraithangam, J., Arumugam, M., Gandhi, E., Chinnaperumal, K., Thirunavukkarasu, S., Sampath, M., Abdul, A. Z., Asokan, B., Chidambaram, J., Arivarasan, V. K., Moorthy, I., Chinnadurai, S., (2013). "Novel and simple approach using synthesized nickel nanoparticles to control blood-sucking parasites", *Vet. Parasitol*., 191: 332-339.
50. Mallikarjuna, K., Narasimha, G., Dillip, G., Praveen, B., Shreedhar, B., Sreelakshmi, C., Reddy, B., Deva, P., (2011). "Green synthesis of silver nanoparticles using ocimum leaf extract and their characterization", *Dig. J. Nanomater. Biostruct*., 6: 181-186.
51. Zhang, H., Ran, X., Wu, X., Zhang, D., (2011). "Evaluation of electro-oxidation of biologically treated landfill leachate using response surface methodology", *J. Hazard. Mater*., 188: 261-268.
52. Iqbal, M., Bhatti, I. A., (2015). "Gamma radiation/$H_2O_2$ treatment of a nonylphenol ethoxylates: Degradation, cytotoxicity, and mutagenicity evaluation", *J. Hazard. Mater*., 299: 351-360.